MDPI

Article

Towards Active Safety Driving: Controller Design of an Active Rear Steering System for Intelligent Vehicles

Peng Hang [1,*] and **Xinbo Chen** [2]

1   Department of Traffic Engineering and Key Laboratory of Road and Traffic Engineering,
     Ministry of Education, Tongji University, Shanghai 201804, China
2   Clean Energy Automotive Engineering Center, Tongji University, Shanghai 201804, China; austin_1@126.com
*   Correspondence: peng.hang@outlook.com

Abstract: To advance the active safety performance for vehicles, especially in extreme conditions, an active rear steering (ARS) control system is designed in this paper. A driver model is established to simulate the driving behaviour of a human driver who is in charge of the front steering control. In the ARS control system, the sliding mode predictive control (SMPC) approach is applied to the ARS controller design based on a 3 degrees of freedom (DoF) nonlinear vehicle model. In the ARS controller design, four kinds of active safety performances are considered, namely, path-tracking performance, handling performance, lateral stability, and rollover prevention. Furthermore, the priority of the four kinds of active safety performance is defined. According to the control priority, an event-triggered mechanism (ETM) is designed to adjust the SMPC controller of the ARS system to address different driving conditions. Finally, two simulation cases are conducted to evaluate the performance of the proposed ARS system. The results show that the ARS system is in favour of the active safety performance advancement for human drivers. Additionally, the comparative simulation indicates that the SMPC algorithm is superior to the fast terminal sliding mode control (FTSMC) algorithm.

Keywords: active safety; active rear steering; sliding mode predictive control; event-triggered mechanism; intelligent vehicle

1. Introduction

With the development of an advanced driver assistant system (ADAS), the active safety of intelligent vehicles has caused widespread concern, especially in extreme and emergency conditions [1]. The active safety control mainly focuses on the lateral stability control [2]. Various techniques have been proposed, including active front steering (AFS), active rear steering (ARS), torque vectoring control (TVC), direct yaw-moment control (DYC), etc. [3–5]. The above techniques can be divided into two types according to the working principle, namely, steering control and drive or brake control. The steering control approach, i.e., AFS and ARS, can directly affect the lateral motion and yaw motion of vehicles, but the drive or brake control approach, i.e., TVC and DYC, must coordinate the longitudinal motion and lateral motion, which increase the control system complexity and create a challenge for the torque allocation algorithm [6,7]. As for the AFS technique, the machine and human driver must address the shared control of the front steering system [8,9]. However, in the ARS technique, a human driver and the machine can independently control the front and rear steering systems [10]. As a result, the technique issue of control authority allocation and conflict resolution does not exist.

ARS technique has been widely studied by many researchers to improve the active safety performance of intelligent vehicles [11]. Based on the vehicle dynamic model, a feed-forward rear steer control strategy is designed to achieve desired vehicle transient lateral dynamics [12]. With the linear control technology and the sliding mode theory, an ARS

system is designed to deal with the steering stability issue in high-speed conditions [13]. In [14], the linear quadratic control approach is applied to the ARS system, and the comparative study indicates that the designed ARS system shows superior lateral stability compared to AFS. The linear quadratic control approach can only address the common conditions. If the lateral tire force enters the nonlinear area, the control performance of the linear model-based approaches will worsen [15]. To address the above issue, a nonlinear triple-step steering controller is designed for the ARS system, which can improve handling stability even if the tire works in an extremely nonlinear region [16]. Based on the nonlinear three degrees of freedom (DoF) four-wheel steering (4WS) vehicle model, a hierarchical control framework is designed for the ARS system, which shows good robustness to address nonlinear disturbances [17]. In [18], a virtual mass-spring-damper system is applied to the ARS controller design, which can deal with the parametric uncertainties. Considering parametric perturbation, unmodelled dynamics, sensor noise and external disturbance, H∞ control theory is used to advance the robustness of the ARS system [19]. Additionally, the active suspension control is combined with the ARS system to enhance active safety in extreme conditions [20].

The above literature only considers the advancement of lateral stability and handling performance. In addition to handling stability, rollover prevention is another active safety performance index [21]. In [22], a novel pulse ARS system is designed to increase both lateral dynamic stability and rollover prevention performance. An integrated dynamic control with steering (IDCS) is proposed, which applies fuzzy logic to ASR controller design, increasing the controllability and stability of the vehicle on slippery roads [23]. To reduce the likelihood of rollover, a bang-bang control strategy is combined with the pulsed active rear steering to advance active safety [24]. In addition to the handling stability and rollover prevention, path tracking is another critical capability for intelligent vehicles. With the equipment of ADAS, intelligent vehicles can easily realize lane keeping, adaptive cruise, and active lane change to reduce the driving burden of human drivers [25], in which path-tracking performance is reflected. With the linear matrix inequality optimization, an ARS system is able to provide lane departure avoidance and lane keeping [26]. Based on model predictive control (MPC), the differential braking control is combined with the ARS system to increase rollover prevention and path-tracking performance [27]. With the application of a nonlinear vehicle dynamic model, the nonlinear MPC approach is applied to the ARS controller design for path tracking [28]. In [29], driver operating limit and actuator physical limit are considered in the MPC-based ARS controller design, which can improve the active safety performance and meanwhile reduce the human driver's workloads. Based on linear-time-varying (LTV) MPC, a cooperative control framework is designed for the human driver and ARS system, which can be adaptive to different drivers [30]. In [31], the sliding mode control (SMC) is combined with the particle swarm optimization (PSO) to address the nonlinear, highly coupled and over-actuated characteristics of the ARS system. In [32], a novel SMC algorithm is applied to the ARS system design, which shows strong robustness to deal with external disturbances and the road friction variation. In addition to MPC and SMC, other advanced control algorithms have been widely used in the mechatronics applications, including fuzzy control [33], fuzzy optimal control [34], and reinforcement learning-based control [35]. In general, SMC can address the system nonlinearity and external disturbances. However, the undesired chattering produced by SMC is a challenge for real application. In this paper, a sliding mode predictive control (SMPC) is proposed for the ARS system design, which integrates the advantages of SMC and MPC, and eliminates the drawbacks of two control algorithms. SMPC can improve the robustness with respect to MPC in the presence of modelling uncertainties and disturbances [36].

Although many studies have been done on the ARS system design to improve the active safety for intelligent vehicles, there still exist some challenges. For instance, the control performance indexes are usually single and not comprehensive, e.g., only focusing on handling stability or path tracking. Additionally, generally, studies seldom comprehen-

sively consider the control balance relationship or priority of path-tracking performance, handling performance, lateral stability and rollover prevention.

This paper presents an ARS system for intelligent vehicles to advance the active safety performance in extreme driving conditions. The contributions of this paper are as follows: (1) The SMPC algorithm is applied to the ARS system control, which shows superior control performance than traditional SMC algorithm, and can adapt to different human drivers; (2) In the control algorithm, four kinds of active safety performance are comprehensively considered including path-tracking performance, handling performance, lateral stability, and rollover prevention; (3) According to the control priority of the four kinds of active safety performance, an event-triggered mechanism (ETM) is designed to adjust the SMPC controller of the ARS system to address different driving conditions.

The rest of this paper is organized as follows. The control system framework is introduced in Section 2. The driver model and the 4WS vehicle model are built in Section 3. In Section 4, the ARS system is designed with the SMPC algorithm. Section 5 shows the simulation analysis and discussion. Finally, Section 6 gives the conclusion of this paper.

2. Control System Framework for Human Driver and ARS System Based on SMPC

To address the issues described in Section 1, the control system framework for human driver and ARS system is proposed. This is illustrated in Figure 1, which mainly consists of two parts, i.e., the driver control module and the ARS control module. In the driver control module, two driver models are built to simulate the experienced driver and inexperienced driver. According to the inputs from the road condition, the driver model outputs the front steering angle to the 4WS vehicle. In the ARS control module, the vehicle model is constructed for controller design. In the ARS control algorithm, four kinds of active safety performance are considered, including path-tracking performance, handling performance, lateral stability and rollover prevention, and the priority of the four kinds of active safety performance is defined. According to the control priority, an event-triggered mechanism is designed to adjust the SMPC controller of the ARS system. With the collaborative control of human driver and the ARS system, the vehicle can advance the active safety performance.
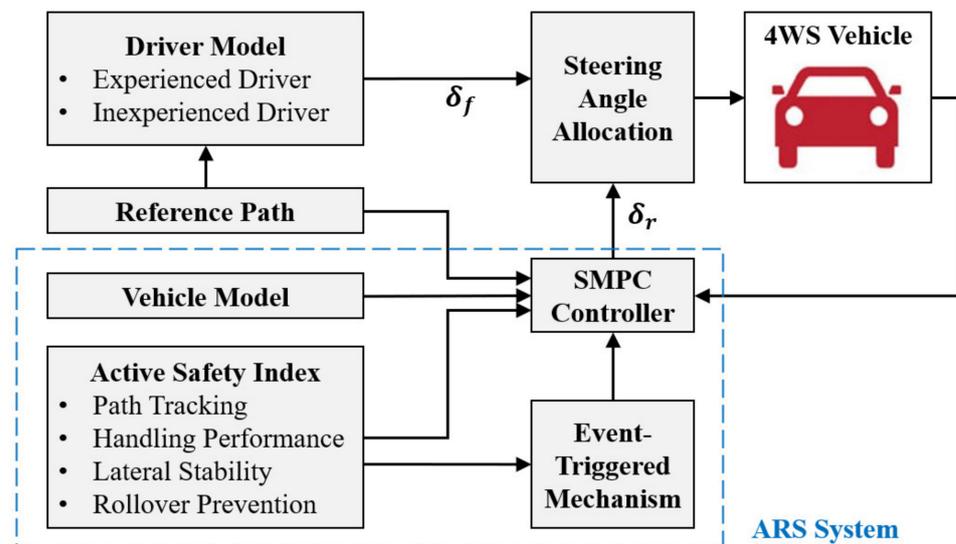
Figure 1. Control system framework of human driver and ARS system.

Some assumptions are made in this paper. In this paper, a common single-point preview driver model is utilized to simulate the human driver. This paper mainly focuses on the lateral safety advancement of vehicles. Thus, a 3 DoF vehicle dynamic model is adopted, which includes lateral, yaw and roll dynamics. The longitudinal motion, pitch motion, and vertical motion are ignored. Besides, to reduce complexity of control algorithm, the above 4-wheel vehicle model is simplified to be a 2-wheel bicycle model.

3. Modelling

3.1. Driver Model

The single-point preview driver model is illustrated in Figure 2. The position coordinate of human driver is $D(X, Y)$. E is the predicted point by human driver in the predicted time τ_p. $P\left(X_p, Y_p\right)$ is the preview position on the target path, which is created by the human driver's eyes. For preview control, the human driver focuses on minimizing the gap between E and P, which includes Δ_1 and Δ_2, $\Delta_1 \approx \tau_p \cdot v_x \varphi$, $\Delta_2 = Y - Y_p$, v_x and φ denote the longitudinal velocity and yaw angle of the vehicle.
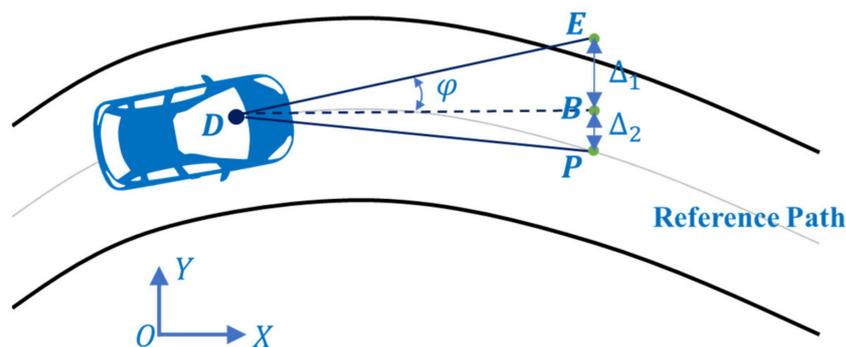

Figure 2. Driver model.

The mathematical description of the single-point preview driver model is shown as follows [37]

$$\ddot{\delta}_f = -\frac{1}{\varrho \tau_d} \dot{\delta}_f - \frac{1}{\varrho \tau_d^2} \delta_f + \frac{\kappa \lambda}{\varrho \tau_d^2} \left[Y_p - \left(Y + \tau_p \cdot v_x \varphi \right) \right] \tag{1}$$

where δ_f denotes the front steering angle, ϱ is associated with the damping rate of the model, τ_d denotes the driver's physical delay time, κ is the transmission ratio of the steering system, and λ is the steering gain.

3.2. 4WS Vehicle Dynamic Model

Figure 3 describes the detailed structure of 4WS vehicle dynamic model, and the model parameters are listed in Table 1. Furthermore, the mathematical expression of the 4WS vehicle dynamic model is derived as follows

$$\begin{cases} mv_x\left(\dot{\beta} + r\right) + m_s h_s \ddot{\phi} = \sum F_y \\ I_z \dot{r} - I_{xz} \ddot{\phi} = \sum M_z \\ I_x \ddot{\phi} - I_{xz} \dot{r} = \sum L_x \end{cases} \tag{2}$$

where β and r denote the sideslip angle and yaw rate at the centre of gravity (CG), ϕ is the roll angle. Besides, $\sum F_y$, $\sum M_z$ and $\sum L_x$ are the total lateral tire force, yaw moment and roll moment acting on the vehicle, which are derived as follows

$$\begin{cases} \sum F_y = F_{yfl} \cos \delta_{fl} + F_{yfr} \cos \delta_{fr} + F_{yrl} \cos \delta_{rl} + F_{yrr} \cos \delta_{rr} \\ \sum M_z = \left(F_{yfl} \cos \delta_{fl} + F_{yfr} \cos \delta_{fr} \right) l_f - \left(F_{yrl} \cos \delta_{rl} + F_{yrr} \cos \delta_{rr} \right) l_r \\ \sum L_x = m_s g h_s \phi - b_\phi \dot{\phi} - k_\phi \phi \end{cases} \tag{3}$$

where δ_i ($i = fl, fr, rl, rr$) denotes the steering angle of each wheel (*fl* denotes the front left wheel, *fr* denotes the front right wheel, *rl* denotes the rear left wheel, and *rr* denotes the rear right wheel). F_{yi} ($i = fl, fr, rl, rr$) denotes the lateral force of each tire. In this paper, Dugoff tire model is used to describe F_{yi}, and the detailed description is shown in [38].
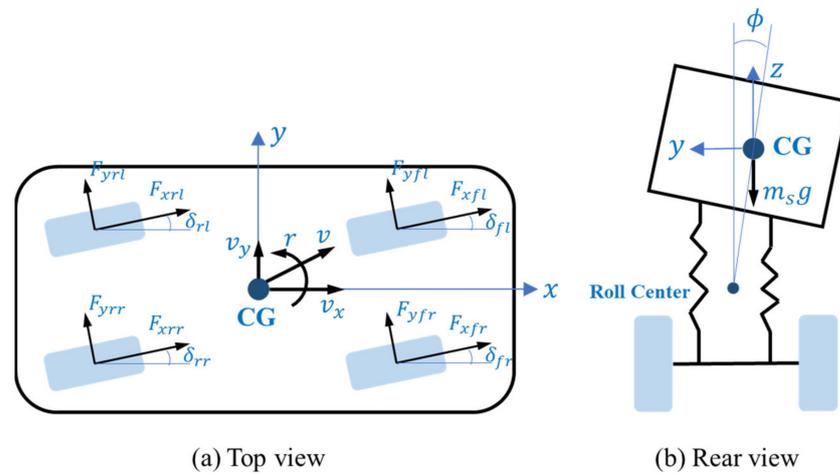
(a) Top view (b) Rear view

Figure 3. 4WS vehicle dynamic model.

Table 1. Parameters of 4WS vehicle.

Parameter	Symbol	Unit	Value
Vehicle mass	m	kg	370
Vehicle sprung mass	m_s	kg	290
Yaw inertia moment	I_z	kg·m^2	217
Roll inertia moment	I_x	kg·m^2	236
The product of inertia	I_{xz}	kg·m^2	152
Front wheel base	l_f	mm	808
Rear wheel base	l_r	mm	726
Wheelbase	l	mm	1534
Height of sprung mass	h_s	mm	430
Track	B	mm	970
Width	B_v	mm	1150
Roll stiffness of vehicle suspension	k_ϕ	N/rad	75,540
Roll damping of vehicle suspension	b_ϕ	N/rad·s	6768
Front tire cornering stiffness	k_f	N/rad	13,007
Rear tire cornering stiffness	kr	N/rad	14,503

Moreover, the motion trajectory description of vehicle is shown as follows

$$\begin{cases} \dot{\varphi} = r \\ \dot{X} = v_x \cos\varphi - v_y \sin\varphi \\ \dot{Y} = v_x \sin\varphi + v_y \cos\varphi \end{cases} \tag{4}$$

where v_x and v_y denote the longitudinal and lateral velocities. X and Y are the position coordinates.

The above 4-wheel vehicle model is then simplified to be a 2-wheel bicycle model, which follow the transformation principle according to Ackerman steering geometry.

$$\begin{aligned} \tan\delta_{fl} &= \frac{\tan\delta_f}{1 - \frac{B}{2l}\left(\tan\delta_f - \tan\delta_r\right)}, \quad \tan\delta_{fr} = \frac{\tan\delta_f}{1 + \frac{B}{2l}\left(\tan\delta_f - \tan\delta_r\right)} \\ \tan\delta_{rl} &= \frac{\tan\delta_r}{1 - \frac{B}{2l}\left(\tan\delta_f - \tan\delta_r\right)}, \quad \tan\delta_{rr} = \frac{\tan\delta_r}{1 + \frac{B}{2l}\left(\tan\delta_f - \tan\delta_r\right)} \end{aligned} \tag{5}$$

where δ_f and δ_r denote the steering angles of front and rear wheels, respectively.

Defining the state vector $x = \begin{bmatrix} \beta & r & \varphi & \phi & \dot{\phi} & Y \end{bmatrix}^T$, and the control vector $u = \delta_r$. The proposed vehicle model can be expressed in the state-space form.

$$\dot{x}(t) = F\left(x(t), u(t), \delta_f(t)\right) \tag{6}$$

$$F\left(x(t), u(t), \delta_f(t)\right) = \begin{bmatrix} -r - \frac{m_s h_s}{m v_x} \ddot{\phi} + \frac{1}{m v_x} \sum F_y \\ \frac{I_{xz}}{I_z} \ddot{\phi} + \frac{1}{I_z} \sum M_z \\ r \\ \dot{\phi} \\ \frac{I_{xz}}{I_x} \dot{r} + \frac{1}{I_x} \sum L_x \\ v_x \sin \varphi + v_y \cos \varphi \end{bmatrix} \tag{7}$$

Furthermore, Equation (6) can be rewritten with a first-order Taylor expansion.

$$\dot{x}(t) = A_t x(t) + B_t u(t) + D_t \delta_f(t) + P_t \tag{8}$$

$$A_t = \left. \frac{\partial F}{\partial x} \right|_{x_t, u_t, \delta_{f,t}}, \quad B_t = \left. \frac{\partial F}{\partial u} \right|_{x_t, u_t, \delta_{f,t}}, \quad D_t = \left. \frac{\partial F}{\partial \delta_f} \right|_{x_t, u_t, \delta_{f,t}} \tag{9}$$

where P_t is the nonlinear disturbance term.

For controller design, Equation (8) is discretized as follows considering parametric uncertainties.

$$\begin{cases} x_{k+1} = (A + \Delta A)x_k + Bu_k + D\delta_{fk} + P_k \\ y_k = Cx_k \end{cases} \tag{10}$$

where $A = e^{A_t T}$, $B = \int_0^T e^{A_t \tau} B_t d\tau$, $D = \int_0^T e^{A_t \tau} D_t d\tau$, ΔA is an uncertain matrix with bounds $\Delta A_{\min} \leq \Delta A \leq \Delta A_{\max}$, T is the sampling time, C is a switch matrix according to the event-triggered mechanism, which will be introduced in Section 4.3.

4. Active Rear Steering System Design

4.1. SMPC Controller

The SMPC controller is designed based on the discrete 4WS vehicle dynamic model, i.e., Equation (10). Firstly, the tracking control error is defined as

$$e_k = y_k - y_k^r \tag{11}$$

where y_k^r is the reference value for tracking.

Based on Equation (11), a linear discrete sliding function is designed as follows

$$s_k = \eta e_k + \Xi_{k-1} \tag{12}$$

$$\Xi_k = \Xi_{k-1} + \eta e_k - \eta C A x_k \tag{13}$$

where the coefficient $\eta > 0$.

In the discrete sliding mode control scheme, the reaching law is defined by

$$\Delta s_k = s_{k+1} - s_k = 0 \tag{14}$$

According to Equation (14), it yields that

$$s_k = s_{k+1} = \eta(y_{k+1} - y_{k+1}^r) + \Xi_k \tag{15}$$

Substitution of y_{k+1} from Equation (10) and Ξ_k from Equation (13) into Equation (15) yields that

$$s_k = \eta \left[C\left(\Delta A x_k + Bu_k + D\delta_{fk} + P_k\right) - y_{k+1}^r \right] + \Xi_{k-1} + \eta e_k \tag{16}$$

Then, the equivalent control law u_k^{eq} can be derived as

$$u_k^{eq} = -(\eta CB)^{-1} \left[\eta C\Delta A x_k + \eta C D\delta_{fk} + \eta C P_{k-1} - \eta y_{k+1}^r + \Xi_{k-1} + \eta e_k \right] \tag{17}$$

To advance the control performance, the nonlinear disturbance P_k can be estimated with the one-step delayed value. The estimated value $\widetilde{P}_k$ is expressed as follows.

$$\widetilde{P}_k = P_{k-1} = x_k - Ax_{k-1} - Bu_{k-1} - D\delta_{fk-1} \tag{18}$$

$\Delta P_k = \widetilde{P}_k - P_k$ is the disturbance estimation error. Furthermore, ΔP_k can be derived as

$$\Delta P_k = P_{k-1} - P_k = A(x_k - x_{k-1}) + B(u_k - u_{k-1}) + D\left(\delta_{fk} - \delta_{fk-1}\right) - (x_{k+1} - x_k) \tag{19}$$

Substitution of Equations (17) and (18) into Equation (10) yields the sliding mode dynamics in the sliding surface $s_k = 0$.

$$x_{k+1} = \left(A + \Delta A - \Delta\hat{A}\right)x_k - B(\eta CB)^{-1}\eta e_k + \sigma_k \tag{20}$$

where $\sigma_k = B(\eta CB)^{-1}\eta y^r_{k+1} - B(\eta CB)^{-1}\Xi_{k-1}$ and $\Delta\hat{A} = B(\eta CB)^{-1}\eta C\Delta A$.

Based on Equation (20), the system stability considering uncertainties ΔA can be proved via linear matrix inequality. The detailed proof is shown in [39], which will not be introduced repeatedly.

According to Equations (10) and (11), it can be derived that

$$e_{k+1} = y_{k+1} - y^r_{k+1} = C(A + \Delta A)x_k + CBu_k + CD\delta_{fk} + CP_k - y^r_{k+1} \tag{21}$$

Substitution of Equation (17) into Equation (21) yields that

$$e_{k+1} = y_{k+1} - y^r_{k+1} = C(P_k - P_{k-1}) - \eta^{-1}\Xi_{k-1} \tag{22}$$

In addition, based on Equation (12), it gives

$$s_{k+1} = \eta e_{k+1} + \Xi_k \tag{23}$$

To improve the control performance, MPC is utilized to drive the system output trajectory onto the sliding surface with an optimal control law u^{mp}_k [40]. Then, the control vector using SMPC can be expressed as

$$u_k = u^{eq}_k + u^{mp}_k \tag{24}$$

Combination of Equations (16), (17), (19), (23) and (24), it is derived that

$$s_{k+1} = s_k + \eta CBu^{mp}_k - \eta C\Delta P_k \tag{25}$$

Defining the prediction horizon and control horizon as N, the prediction of the sliding function at the time step $k + N$ can be derived as

$$s_{k+N} = s_k + \eta CB\sum_{p=0}^{k+N-1} u^{mp}_{k+p} - \eta C\sum_{p=0}^{k+N-1} \Delta P_{k+p} \tag{26}$$

Combination of all predicted sliding functions yields that

$$\mathbf{s}_k = \Gamma s_k + \Theta\mathbf{u}_{k-1} - \Omega\mathbf{P}_{k-1} \tag{27}$$

where

$$\mathbf{s}_k = [s_{k+1}, s_{k+2}, \cdots, s_{k+N}]^T \tag{28}$$

$$\mathbf{u}_{k-1} = \left[u^{mp}_k, u^{mp}_{k+1}, \cdots, u^{mp}_{k+N-1}\right]^T \tag{29}$$

$$\mathbf{P}_{k-1} = [\Delta P_k, \Delta P_{k+1}, \cdots, \Delta P_{k+N-1}]^T \tag{30}$$

Additionally, $\Gamma = I_{N \times 1}$, Θ and Ω are lower triangular matrices with nonzero elements of ηCB and ηC.

To obtain the control sequence $\mathbf{u}_{k-1}$, a cost function is designed as

$$J = \mathbf{s}_k^T \mathbf{s}_k + \xi \mathbf{u}_{k-1}^T \mathbf{u}_{k-1} \tag{31}$$

where ξ denotes the weighting coefficient.

The necessary condition to minimize J is equivalent to

$$\frac{\partial J}{\partial \mathbf{u}_{k-1}} = 0 \tag{32}$$

It yields that

$$\mathbf{u}_{k-1} = -\left(\Theta^T \Theta + \xi I\right)^{-1} \Theta^T \left(\Gamma s_k - \Omega \mathbf{P}_{k-1}\right) \tag{33}$$

where $\mathbf{P}_{k-1}$ is estimated.

$$\tilde{\mathbf{P}}_{k-1} = [\Delta P_k, \Delta P_{k+1}, \cdots, \Delta P_{k+N-1}]^T \tag{34}$$

Choosing the first element of the control sequence $\mathbf{u}_{k-1}$ as the control action, it gives

$$u_k^{mp} = -e\left(\Theta^T \Theta + \xi I\right)^{-1} \Theta^T \left(\Gamma s_k - \Omega \mathbf{P}_{k-1}\right) \tag{35}$$

where $e = [1, 0, 0, \cdots, 0]$.

Finally, the control vector u_k can be expressed as with the sum of Equations (17) and (35).

To prove the stability of the close-loop control system, substitution of Equations (33) and (34) into Equation (27), it yields that

$$\mathbf{s}_k = \Gamma s_k - \Theta\left(\Theta^T \Theta + \xi I\right)^{-1} \Theta^T \left(\Gamma s_k - \Omega \tilde{\mathbf{P}}_{k-1}\right) - \Omega \mathbf{P}_{k-1} \tag{36}$$

Assuming that there is no penalty for the control effect, i.e., $\xi = 0$, Equation (36) can be derived as

$$\mathbf{s}_k = \Omega\left(\tilde{\mathbf{P}}_{k-1} - \mathbf{P}_{k-1}\right) \tag{37}$$

Taking out the first element of the predicted sliding functions $\mathbf{s}_k$, and considering Equations (28) and (34), it can be obtained that

$$s_{k+1} = \eta C(\Delta P_{k-1} - \Delta P_k) = \eta C(P_k - 2P_{k-1} + P_{k-2}) \tag{38}$$

Since the disturbance change rate ΔP_k is bounded, it can be derived that

$$|s_{k+1}| \leq \Delta_s \tag{39}$$

where Δ_s is defined as the quasi-sliding mode band width [39].

According to the definition of quasi-sliding mode control in [41], it can be concluded that the closed-loop system satisfies the reaching condition of the quasi-sliding mode in Δ_s vicinity of the sliding surface in a finite number of steps. Therefore, the control system is stable.

4.2. Active Safety Performance

Four kinds of active safety performance are considered in this paper including path-tracking performance, handling performance, lateral stability, and rollover prevention.

The path-tracking performance is mainly reflected by the lateral offset ΔY. The smaller the lateral offset, the better the path-tracking performance. The boundary of ΔY is defined by

$$|\Delta Y| \leq \Delta Y_{max} \tag{40}$$

where ΔY_{max} denotes the maximum lateral offset.

The handling performance of vehicles is evaluated by yaw rate r. The limit of yaw rate is related to the longitudinal velocity v_x and the lateral road adhesion coefficient μ_y, which is expressed as

$$|r| \leq r_{max} = \frac{g\mu_y}{v_x} \tag{41}$$

Besides, the lateral stability of vehicles is usually reflected by the sideslip angle β. Small value of β means good lateral stability. The boundary of β is defined by the following empirical formula [42].

$$|\beta| \leq \beta_{max} = \arctan(0.02\,\mu g) \tag{42}$$

Moreover, the performance of rollover prevention is associate with the value of roll angle. The maximum roll angle is defined by the following empirical formula [43].

$$|\phi| \leq \phi_{max} = \frac{Bm_s}{2(k_\phi - m_s g h_s)} \tag{43}$$

4.3. Event-Triggered Control

For active safety control, the priority of the four performance indexes is defined as follows: path-tracking performance < handling performance < lateral stability < rollover prevention. In common conditions, the vehicle will not reach the boundaries of lateral stability and rollover prevention. Therefore, path tracking is the main task. However, in extreme conditions, e.g., emergent collision avoidance and icy road condition, lateral stability advancement and rollover prevention are the focus.

According to different control objectives, i.e., the four performance indexes, the matrix C will be changeable, which results in different SMPC controllers.

$$u_k = \begin{cases} u_k^{pt}, & C = [0,\,0,\,0,\,0,\,0,\,1] \\ u_k^{hp}, & C = [0,\,1,\,0,\,0,\,0,\,0] \\ u_k^{ls}, & C = [1,\,0,\,0,\,0,\,0,\,0] \\ u_k^{rp}, & C = [0,\,0,\,0,\,1,\,0,\,0] \end{cases} \tag{44}$$

where u_k^{pt}, u_k^{hp}, u_k^{ls}, and u_k^{rp} denote the controllers of path tracking, handling performance, lateral stability, and rollover prevention.

The event-triggered mechanism (ETM) of four controllers is defined as follows

$$t_{k+1} \triangleq \inf\{t > t_k | |\mathcal{H}|\rangle \mathcal{H}_{max}\} \tag{45}$$

where $\mathcal{H}$ denotes ΔY, r, β, and ϕ.

Equation (45) indicates that once the control performance index is beyond its boundary, the corresponding controller will be triggered. Additionally, the ETM should follow the priority setting of the four control performance indexes. In this case that all performance indexes are in their boundaries, based on Equation (44), the four controllers for path tracking, handling performance, lateral stability, and rollover prevention are calculated, respectively. Then, the integrated controller is obtained by the weighted distribution of the four controllers, i.e.,

$$u_k = \omega^{pt} u_k^{pt} + \omega^{hp} u_k^{hp} + \omega^{ls} u_k^{ls} + \omega^{rp} u_k^{rp} \tag{46}$$

where ω^{pt}, ω^{hp}, ω^{ls}, and ω^{rp} are the weighting coefficients. $\omega^{pt} = q^{pt}/\left(q^{pt} + q^{hp} + q^{ls} + q^{rp}\right)$, $\omega^{hp} = q^{hp}/\left(q^{pt} + q^{hp} + q^{ls} + q^{rp}\right)$, $\omega^{ls} = q^{ls}/\left(q^{pt} + q^{hp} + q^{ls} + q^{rp}\right)$, $\omega^{rp} = q^{rp}/\left(q^{pt} + q^{hp} + q^{ls} + q^{rp}\right)$, $q^{pt} = |\Delta Y|/\Delta Y_{max}$, $q^{hp} = |r|/r_{max}$, $q^{ls} = |\beta|/\beta_{max}$, $q^{rp} = |\phi|/\phi_{max}$.

5. Simulation Results and Discussion

In this section, the effectiveness and feasibility of the proposed ARS system are verified with two cases based on the Simulink simulation platform. Figure 4 shows the Simulink algorithm structure in the simulation platform, including the human driver model, the SMPC algorithm in the ARS system module, the longitudinal motion control algorithm and the braking control algorithm. All control algorithms are carried out in Simulink software. The controller parameters for simulation are shown in Table 2. The real 4WS intelligent vehicle is simulated with the 14 DoF vehicle model.
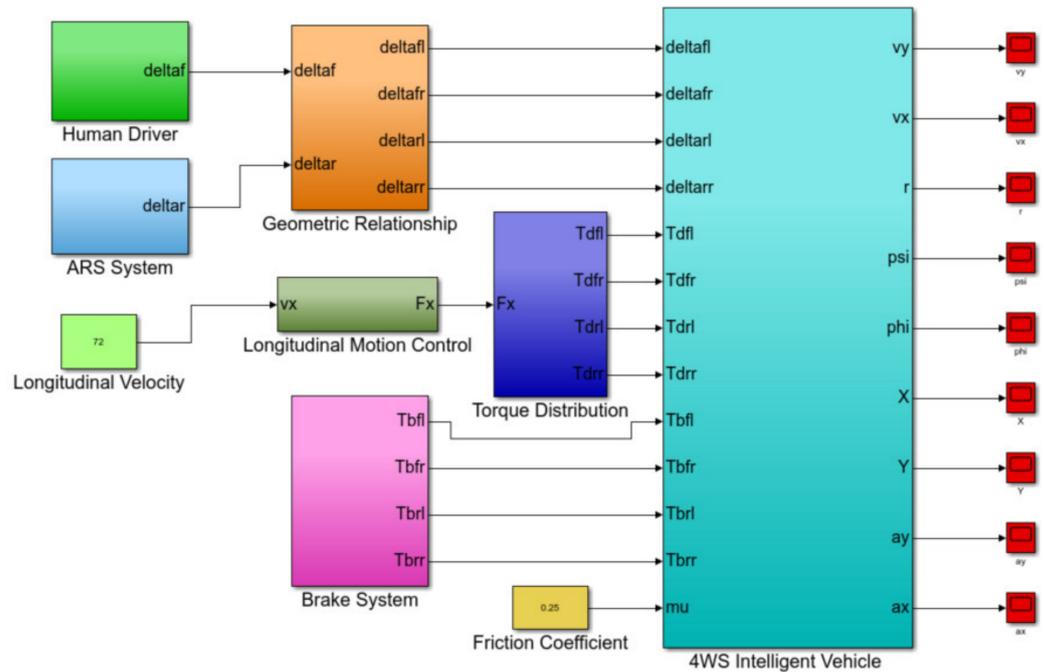

Figure 4. Simulation platform for algorithm verification.

Table 2. Controller parameters for simulation.

Parameter	Value	Parameter	Value
$\Delta Y_{\max}$(m)	0.5	N	10
$\Delta A_{\max}$	$0.1A$	η	2
$\Delta A_{\min}$	$-0.1A$	T(s)	0.001

To conduct comparative simulation, two kinds of driver model are built to simulate the experienced driver and the inexperienced driver. Referring to [30], the parameters of the two driver models are described in Table 3, where Driver 1 denotes the inexperienced driver and Driver 2 denotes the experienced driver. Moreover, the comparative simulation of the SMPC-based ARS system and the FTSMC-based ARS system is carried out to evaluate the superiority of the SMPC algorithm.

Table 3. Parameters of driver model.

| Parameter	Driver 1	Driver 2
τ_d	0.24	0.14
τ_p	0.83	1.02
λ	0.62	0.84
ϱ	0.22	0.24

5.1. Case Study A

The first case is a double lane-change (DLC) scenario. The longitudinal velocity is set as 20 m/s and the road adhesion coefficient is set as 0.25 to simulate the icy road condition, which can be regarded as an extreme condition for algorithm verification. Both the experienced driver and the inexperienced driver are considered in this case. The proposed ARS system will be used to advance the two drivers' driving safety.

The simulation results of vehicle moving trajectories are illustrated in Figure 5, from which we can see that Driver 1 has the largest path-tracking error due to the lack of driving experience. The lateral offset is shown in Figure 6a. The lateral offset of Driver 1 has exceeded the maximum value. However, with the assistance of ARS system, both Driver 1 and Driver 2 can improve the path-tracking performance. Additionally, the simulation results of sideslip angle, yaw rate and roll angle are depicted in Figure 6b–d, respectively. It can be seen that, although Driver 2 is an experienced driver, he/she cannot guarantee the handling stability of the vehicle. With the application of ARS system, the values of sideslip angle, yaw rate and roll angle are decreased remarkably, which shows the capability of ARS system to advance active safety performance. Additionally, Figure 7 shows the front and rear steering angles of AVs in Case A. Without the assistance of ARS system, both the front steering angles of Driver 1 and Driver 2 are not convergent, which results in the loss of stability control.
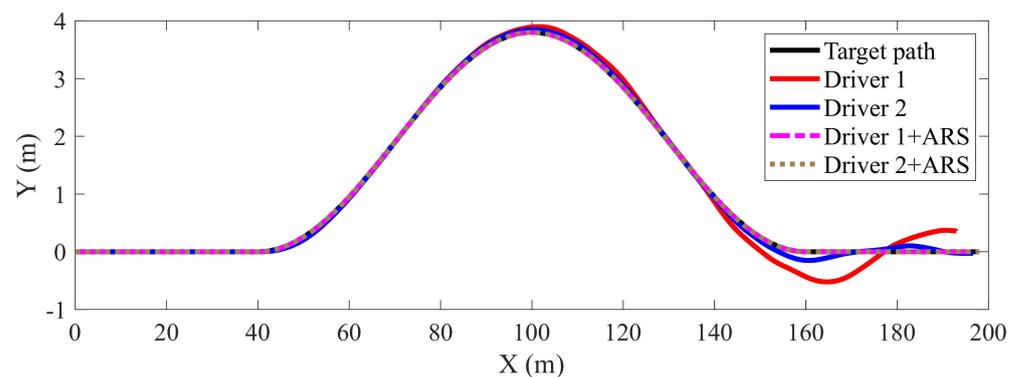

Figure 5. Moving trajectories of vehicles in Case A.

Table 4 shows the maximum control error analysis of four kinds of active safety performances, which also supports the conclusion drawn according to Figures 5 and 6. In Table 4, ↓ means the performance index is decreased. With the ARS system, the control errors of four kinds of active safety performance indexes are decreased remarkably in extreme driving conditions, which verifies the effectiveness of the proposed SMPC algorithm.
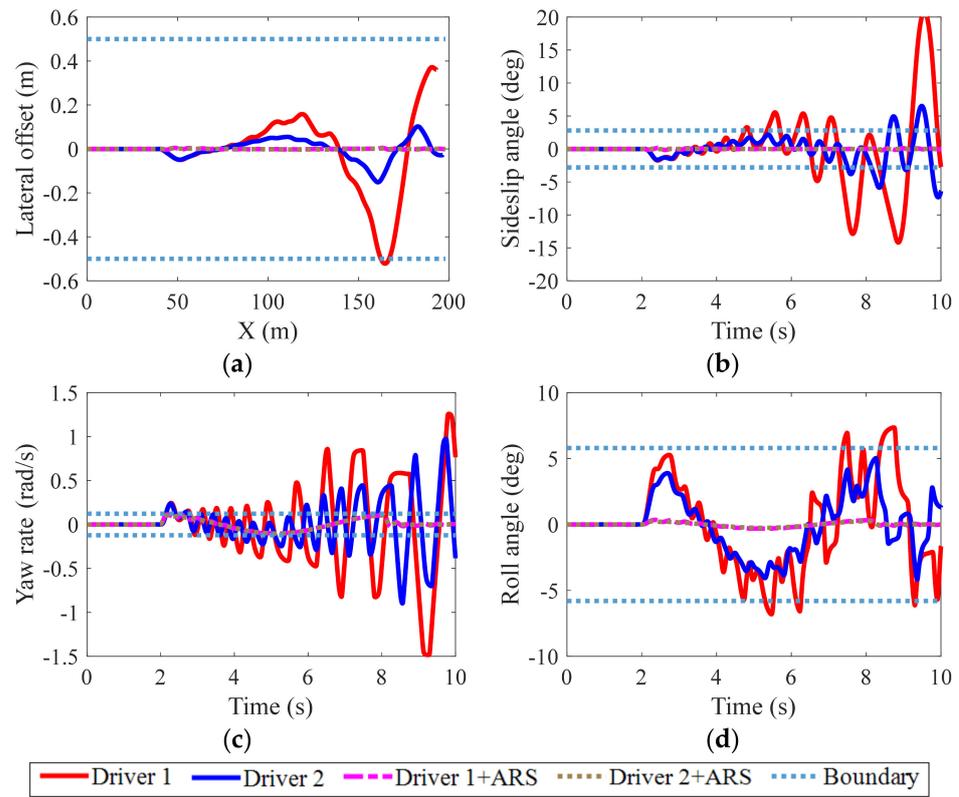
Figure 6. Active safety performances of vehicles in Case A: (**a**) lateral offset; (**b**) sideslip angle; (**c**) yaw rate: (**d**) roll angle.
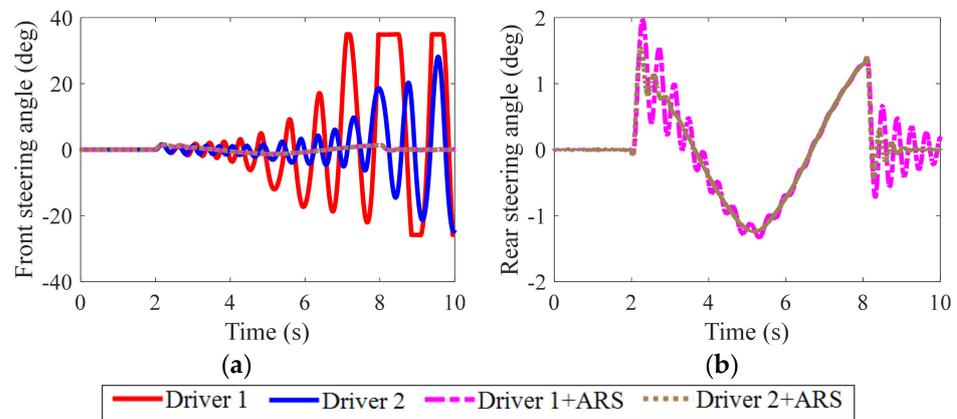

Figure 7. Front and rear steering angles of vehicles in Case A: (**a**) front steering angle; (**b**) rear steering angle.

Table 4. Maximum control errors of active safety performances in Case A.

Control Mode	Lateral Offset (m)	Sideslip Angle Error (deg)	Yaw Rate Error (rad/s)	Roll Angle Error (deg)
Driver 1	0.5217	20.7762	1.4848	7.3549
Driver 1 + ARS	0.0049 (↓)	0.1878 (↓)	0.0269 (↓)	0.3501 (↓)
Driver 2	0.1514	7.3190	0.9739	5.0298
Driver 2 + ARS	0.0027 (↓)	0.0940 (↓)	0.0105 (↓)	0.2572 (↓)

Additionally, the algorithm efficiency is evaluated. Figure 8 shows the computational time of the proposed algorithm with ETM and without ETM. Without ETM, the mean value of the computational time at each time step is 0.0078 s. However, with the application of ETM, the mean value of the computational time at each time step is 0.0051 s. It indicates that ETM can improve the algorithm efficiency.
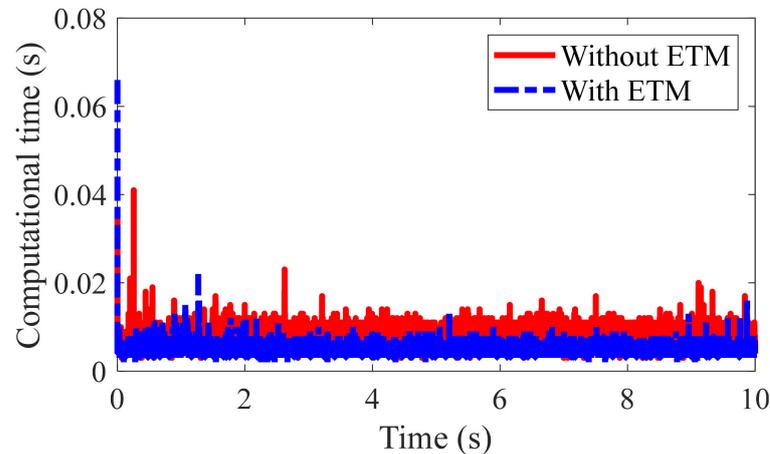
Figure 8. Computational time.

5.2. Case Study B

This case mainly focuses on the comparative performance verification of the proposed SMPC algorithm, and FTSMC algorithm which is a common SMC scheme not using prediction. The longitudinal velocity is set as 25 m/s and the road adhesion coefficient is set as 0.5 to simulate the wet road condition. The simulation case is a S-shape turn scenario, which can also be regarded as an extreme condition. To show the superiority of the ARS system, only an inexperienced driver (Driver 1) is considered in this case.

The path-tracking results of vehicles are displayed in Figure 9. Due to the large-curvature path, Driver 1 cannot conduct good path tracking. Additionally, we can see that both ARS1 (FTSMC based) and ARS2 (SMPC based) can guarantee the path-tracking performance. The lateral offset is depicted in Figure 10a. We can see that the lateral offset of Driver 1 has exceeded the maximum boundary. The lateral offsets of ARS1 and ARS2 are very small, which indicates the superiority of ARS system on path tracking. Figure 10b shows the sideslip angle results, from which we can see the vehicle controlled by human driver has lost stability. The results of yaw angle and roll angle of the vehicle controlled by human driver are also beyond the safe boundary, which indicates the driving safety of vehicle is terrible. To see the detailed comparative results of ARS1 and ARS2, Table 5 shows the maximum control errors of the four kinds of active safety performance indexes. It can be seen that both ARS1 and ARS2 can decrease the control error of path tracking, handling performance, lateral stability and rollover prevention, but ARS2 shows superior capability to guarantee the handling stability and rollover prevention.

Table 5. Maximum control errors of active safety performances in Case B.

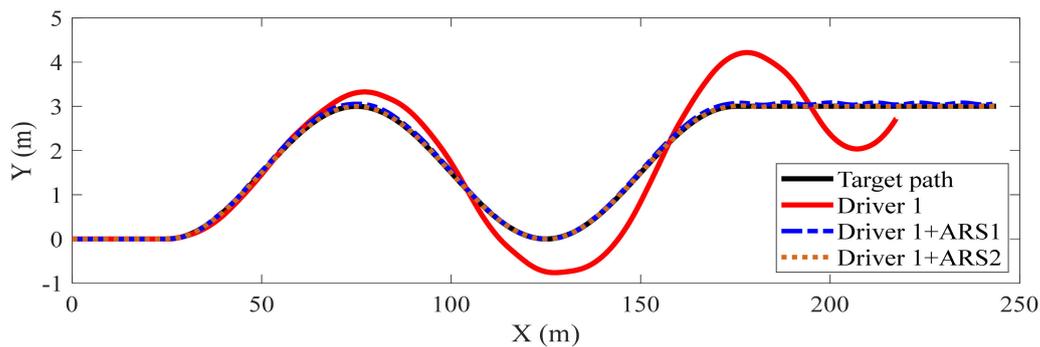| Control Mode	Lateral Offset (m)	Sideslip Angle Error (deg)	Yaw Rate Error (rad/s)	Roll Angle Error (deg)
Driver 1	1.4129	46.7191	2.1428	7.2451
Driver 1 + ARS1	0.0284 ($\downarrow$)	2.4067 ($\downarrow$)	0.2234 ($\downarrow$)	1.7615 ($\downarrow$)
Driver 1 + ARS2	0.0174 ($\downarrow\downarrow$)	1.5475 ($\downarrow\downarrow$)	0.0504 ($\downarrow\downarrow$)	0.4449 ($\downarrow\downarrow$)

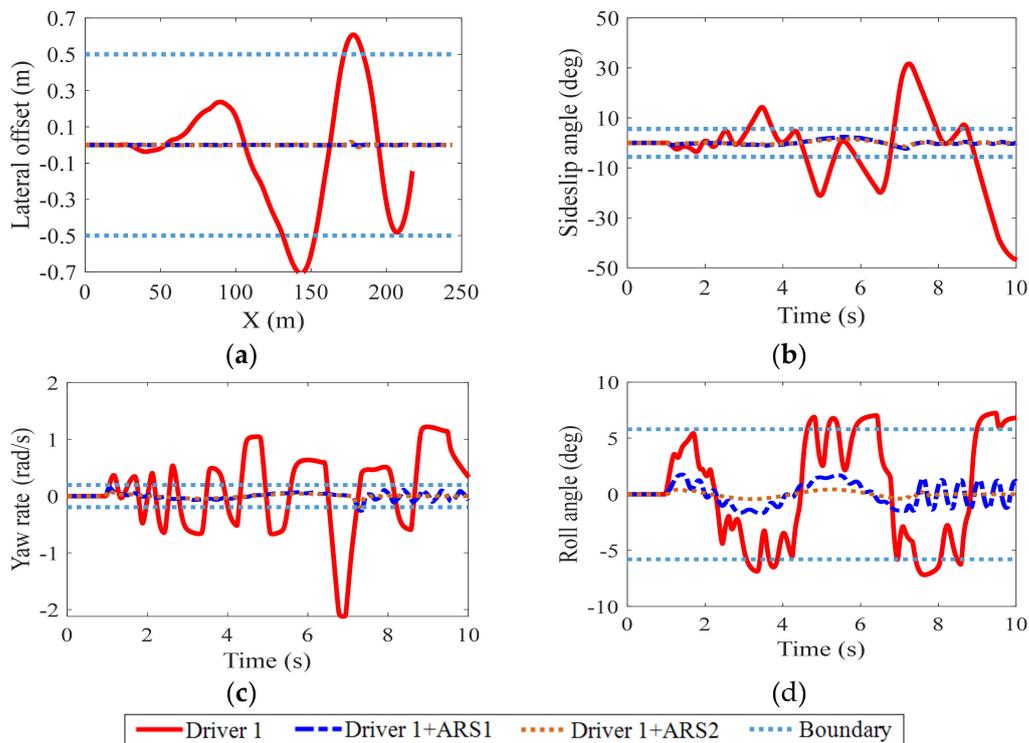**Figure 9.** Moving trajectories of vehicles in Case B.

Figure 10. Active safety performances of vehicles in Case B: (**a**) lateral offset; (**b**) sideslip angle; (**c**) yaw rate: (**d**) roll angle.

Additionally, the front and rear steering angles of vehicles are displayed in Figure 11. We can see that the front steering angle of Driver 1 has exceeded the maximum boundary and cannot converge to the steady value, which indicates that human driver has lost the effective control of the vehicle. From Figure 11b, we can see that the rear steering angle of ARS1 is always oscillating in the control process. The controller jitter issue of ARS1 cannot be addressed. However, it can be seen that there is no obvious controller jitter in the control process of ARS2.
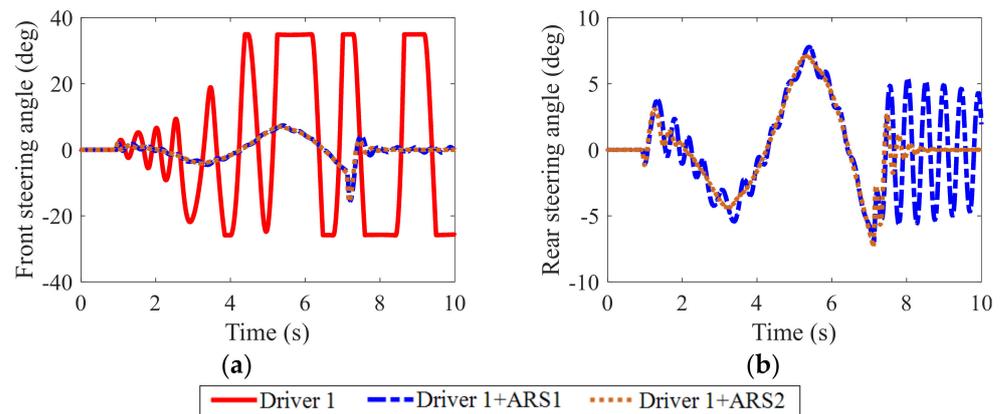
Figure 11. Front and rear steering angles of vehicles in Case B: (**a**) front steering angle; (**b**) rear steering angle.

5.3. Discussion

From the results of above two simulation cases, we can conclude that compared with existing ARS control algorithms, the proposed ARS control algorithm can comprehensively consider multiple performances of active safety, and can adapt to different human drivers. In addition, the ETM-based control framework is able to balance the control weighting of path-tracking performance, handling performance, lateral stability and rollover prevention, which can avoid the waste of control resources. Although both ARS1 and ARS2 can advance the active safety performance of vehicles in extreme conditions, the SMPC-based ARS (ARS2) system shows better capability to deal with handling stability and rollover prevention. Additionally, the controller jitter issue of traditional SMC approach can be addressed with the SMPC approach. To summarize, the comparative simulation results can demonstrate the superiority of the proposed ARS control algorithm and framework.

6. Conclusions and Future Work

The paper presents an ARS system for intelligent vehicles to advance the active safety performance. The human driver is simulated with a single-point preview driver model, which outputs the front steering angle to the vehicle. A 3 DoF nonlinear vehicle model is built for the ARS controller design. Based on the vehicle model, SMPC approach is applied to the ARS controller design. In the control algorithm, four kinds of active safety performance are considered including path-tracking performance, handling performance, lateral stability and rollover prevention, and the priority of the four kinds of active safety performance is defined. According to the control priority, an event-triggered mechanism is designed to adjust the SMPC controller of the ARS system. To evaluate the performance of the ARS system, two simulation cases are designed and conducted. The results show that the ARS system can improve the active safety performance for both experienced and inexperienced drivers, indicating that the ARS system can adapt to different drivers. Additionally, the proposed ETM-based control framework is able to establish a good balance between different active safety performances. Compared with the conventional SMC algorithm, the SMPC algorithm shows superior control performance.

In future work, the experimental validation of the proposed algorithm will be conducted with real vehicle.

Conflicts of Interest: The authors declare no conflict of interest.

References

1. Hang, P.; Lv, C.; Huang, C.; Xing, Y.; Hu, Z. Cooperative decision making of connected automated vehicles at multi-lane merging zone: A coalitional game approach. *IEEE Trans. Intell. Transp. Syst.* **2021**, *23*, 3829–3841. [CrossRef]
2. Hang, P.; Huang, C.; Hu, Z.; Lv, C. Driving Conflict Resolution of Autonomous Vehicles at Unsignalized Intersections: A Differential Game Approach. *IEEE/ASME Trans. Mechatron.* **2022**. [CrossRef]
3. Doumiati, M.; Sename, O.; Dugard, L.; Martinez-Molinaa, J.-J.; Gasparb, P.; Szabo, Z. Integrated vehicle dynamics control via coordination of active front steering and rear braking. *Eur. J. Control.* **2013**, *19*, 121–143. [CrossRef]
4. Ahmadian, N.; Khosravi, A.; Sarhadi, P. Integrated model reference adaptive control to coordinate active front steering and direct yaw moment control. *ISA Trans.* **2020**, *106*, 85–96. [CrossRef] [PubMed]
5. Song, J. Integrated vehicle dynamic controls using active rear wheel steering and four wheel braking. *Int. J. Veh. Syst. Model. Test.* **2018**, *13*, 26–43.
6. Peng, H.; Chen, X. Active Safety Control of X-by-Wire Electric Vehicles: A Survey. *SAE Int. J. Veh. Dyn. Stab. NVH* **2022**, *6*, 115–133. [CrossRef]
7. Ye, Z.; Xie, W.; Yin, Y.; Fu, Z. Dynamic rollover prediction of heavy vehicles considering critical frequency. *Automot. Innov.* **2020**, *3*, 158–168. [CrossRef]
8. Aouadj, N.; Hartani, K.; Fatiha, M. New integrated vehicle dynamics control system based on the coordination of active front steering, direct yaw control, and electric differential for improvements in vehicle handling and stability. *SAE Int. J. Veh. Dyn. Stab. NVH* **2020**, *4*, 119–133. [CrossRef]
9. Xue, W.; Zheng, L. Active collision avoidance system design based on model predictive control with varying sampling time. *Automot. Innov.* **2020**, *3*, 62–72. [CrossRef]
10. Vignati, M.; Sabbioni, E. A cooperative control strategy for yaw rate and sideslip angle control combining torque vectoring with rear wheel steering. *Veh. Syst. Dyn.* **2021**, *60*, 1668–1701. [CrossRef]
11. Pan, K.; Zheng, H.; Wu, J.; Xiao, H. Research on Steering Control of Multi-Axle Steering Heavy Commercial Vehicle Based on Reducing Tire Wear. *SAE Int. J. Veh. Dyn. Stab. NVH* **2020**, *4*, 67–80.
12. Bredthauer, L.; Lynch, D. Use of active rear steering to achieve desired vehicle transient lateral dynamics. SAE Technical Paper. 2018. Available online: https://saemobilus.sae.org/content/2018-01-0565/ (accessed on 14 June 2022).
13. Zhang, J.; Zheng, H.; Zhao, M. Analysis of Vehicle Steering Stability of Nonlinear Four Wheel Steering Based on Sliding Mode Control. SAE Technical Paper. 2018. Available online: https://saemobilus.sae.org/content/2018-01-1593/ (accessed on 14 June 2022).
14. Zhang, Z.; Huang, M.; Ji, M.; Zhu, S. Design of the linear quadratic control strategy and the closed-loop system for the active four-wheel-steering vehicle. *SAE Int. J. Passeng. Cars-Mech. Syst.* **2015**, *8*, 354–363. [CrossRef]
15. Hang, P.; Lou, B.; Lv, C. Nonlinear Predictive Motion Control for Autonomous Mobile Robots Considering Active Fault-Tolerant Control and Regenerative Braking. *Sensors* **2022**, *22*, 3939. [CrossRef]
16. Yu, S.; Li, W.; Wang, W.; Qu, T. Nonlinear control of active four wheel steer-by-wire vehicles. *IEEE Access* **2019**, *7*, 127117–127127. [CrossRef]
17. Tian, J.; Ding, J.; Tai, Y.; Chen, N. Hierarchical control of nonlinear active four-wheel-steering vehicles. *Energies* **2018**, *11*, 2930. [CrossRef]
18. Kreutz, M.; Horn, M.; Zehetner, J. Improving vehicle dynamics by active rear wheel steering systems. *Veh. Syst. Dyn.* **2009**, *47*, 1551–1564. [CrossRef]
19. Hang, P.; Xia, X.; Chen, X. Handling stability advancement with 4WS and DYC coordinated control: A gain-scheduled robust control approach. *IEEE Trans. Veh. Technol.* **2021**, *70*, 3164–3174. [CrossRef]
20. Wu, L.; Ma, F.; Pu, Y.; Yin, H. Integrated Effects of Active Suspension and Rear-Wheel Steering Control Systems on Vehicle Lateral Stability. SAE Technical Paper. 2017. Available online: https://saemobilus.sae.org/content/2017-01-0257/ (accessed on 14 June 2022).
21. Zhou, Z.; Huang, M.; Zhao, Y.; Fang, C. Vehicle Stability Control through Optimized Coordination of Active Rear Steering and Differential Driving/Braking. *SAE Int. J. Passeng. Cars-Mech. Syst.* **2018**, *11*, 239–248. [CrossRef]
22. Zhang, B.; Khajepour, A.; Goodarzi, A. Vehicle yaw stability control using active rear steering: Development and experimental validation. *Proc. Inst. Mech. Eng. Part K J. Multi-Body Dyn.* **2017**, *231*, 333–345. [CrossRef]
23. Song, J. Integrated control of brake pressure and rear-wheel steering to improve lateral stability with fuzzy logic. *Int. J. Automot. Technol.* **2012**, *13*, 563–570. [CrossRef]
24. Zhang, Y.; Khajepour, A.; Xie, X. Rollover prevention for sport utility vehicles using a pulsed active rear-steering strategy. *Proc. Inst. Mech. Eng. Part D J. Automob. Eng.* **2016**, *230*, 1239–1253. [CrossRef]
25. Hang, P.; Chen, X. Towards Autonomous Driving: Review and Perspectives on Configuration and Control of Four-Wheel Independent Drive/Steering Electric Vehicles. *Actuators* **2021**, *10*, 184. [CrossRef]
26. Enache, N.M.; Guegan, S.; Desnoyer, F.; Vorobieva, H. Lane keeping and lane departure avoidance by rear wheels steering. In Proceedings of the 2012 IEEE Intelligent Vehicles Symposium, Alcala de Henares, Spain, 3–7 June 2012; pp. 359–364.
27. Lee, S.; Yakub, F.; Kasahara, M.; Mori, Y. Rollover prevention with predictive control of differential braking and rear wheel steering. In Proceedings of the 6th IEEE Conference on Robotics, Automation and Mechatronics (RAM), Manila, Philippines, 12–15 November 2013; pp. 144–149.

28. Yu, C.; Zheng, Y.; Shyrokau, B.; Ivanov, V. MPC-based path following design for automated vehicles with rear wheel steering. In Proceedings of the 2021 IEEE International Conference on Mechatronics (ICM), Chiba, Japan, 7–9 March 2021; pp. 1–6.

29. Zhang, H.; Heng, B.; Zhao, W. Path Tracking Control for Active Rear Steering Vehicles Considering Driver Steering Characteristics. *IEEE Access* **2020**, *8*, 98009–98017. [CrossRef]

30. Hang, P.; Chen, X.; Wang, W. Cooperative control framework for human driver and active rear steering system to advance active safety. *IEEE Trans. Intell. Veh.* **2021**, *6*, 460–469. [CrossRef]

31. Dai, P.; Katupitiya, J. Force control for path following of a 4WS4WD vehicle by the integration of PSO and SMC. *Veh. Syst. Dyn.* **2018**, *56*, 1682–1716. [CrossRef]

32. Wu, Y.; Li, B.; Zhang, N.; Du, H.; Zhang, B. Rear-steering based decentralized control of four-wheel steering vehicle. *IEEE Trans. Veh. Technol.* **2020**, *69*, 10899–10913. [CrossRef]

33. Precup, R.E.; Preitl, S. Stability and sensitivity analysis of fuzzy control systems. Mechatronics applications. *Acta Polytech. Hung.* **2006**, *3*, 61–76.

34. Chen, T.; Babanin, A.; Muhammad, A.; Chapron, B.; Chen, C. Modified evolved bat algorithm of fuzzy optimal control for complex nonlinear systems. *Rom. J. Inf. Sci. Technol.* **2020**, *23*, 28–40.

35. Zamfirache, I.A.; Precup, R.E.; Roman, R.C.; Petriu, E.M. Policy iteration reinforcement learning-based control using a grey wolf optimizer algorithm. *Inf. Sci.* **2022**, *585*, 162–175. [CrossRef]

36. Huang, C.; Naghdy, F.; Du, H. Fault tolerant sliding mode predictive control for uncertain steer-by-wire system. *IEEE Trans. Cybern.* **2017**, *49*, 261–272. [CrossRef]

37. Zhou, X.; Jiang, H.; Li, A.; Ma, S. A New Single Point Preview-Based Human-Like Driver Model on Urban Curved Roads. *IEEE Access* **2020**, *8*, 107452–107464. [CrossRef]

38. Hang, P.; Xia, X.; Chen, G.; Chen, X. Active safety control of automated electric vehicles at driving limits: A tube-based MPC approach. *IEEE Trans. Transp. Electrif.* **2022**, *8*, 1338–1349. [CrossRef]

39. Huang, C.; Naghdy, F.; Du, H. Sliding mode predictive tracking control for uncertain steer-by-wire system. *Control. Eng. Pract.* **2019**, *85*, 194–205. [CrossRef]

40. Xu, Q. Digital integral terminal sliding mode predictive control of piezoelectric-driven motion system. *IEEE Trans. Ind. Electron.* **2015**, *63*, 3976–3984. [CrossRef]

41. Bartoszewicz, A. Discrete-time quasi-sliding-mode control strategies. *IEEE Trans. Ind. Electron.* **1998**, *45*, 633–637. [CrossRef]

42. Yue, M.; Yang, L.; Sun, X.M.; Xia, W. Stability control for FWID-EVs with supervision mechanism in critical cornering situations. *IEEE Trans. Veh. Technol.* **2018**, *67*, 10387–10397. [CrossRef]

43. Ataei, M.; Khajepour, A.; Jeon, S. Model Predictive Control for integrated lateral stability, traction/braking control, and rollover prevention of electric vehicles. *Veh. Syst. Dyn.* **2020**, *58*, 49–73. [CrossRef]